CHEMISTRY
A EUROPEAN JOURNAL

DOI: 10.1002/chem.201102325

In Situ Scanning Electrochemical Microscopy (SECM) Detection of Metal Dissolution during Zinc Corrosion by Means of Mercury Sphere-Cap Microelectrode Tips

Ricardo M. Souto,*[a] Yaiza González-García,[a] Dario Battistel,[b] and Salvatore Daniele*[b]

Abstract: This work presents a scanning electrochemical microscopy (SECM)-based in situ corrosion probing methodology that is capable of monitoring the release of zinc species in corrosion processes. It is based on the use of Hg-coated Pt microelectrodes as SECM tips, which offer a wider negative potential range than bare platinum or other noble-metal tips. This allows for the reduction of zinc ions at the tip to be investigated with low interference from hydrogen evolution and oxygen reduction from aqueous solutions. The processes involved in the corrosion of zinc during its immersion in chloride-containing solutions were successfully monitored by scanning the SECM tip, set at an adequate potential, across the sample either in one direction or in the *X*–*Y* plane parallel to its surface. In this way, it was possible to detect the anodic and cathodic sites at which the dissolution of zinc and the reduction of oxygen occurred, respectively. Additionally, cyclic voltammetry (CV) or constant potential measurements were used to monitor the release of zinc species collected at the tip during an SECM scan.

Keywords: corrosion · cyclic voltammetry · mercury · scanning electrochemistry · zinc

Introduction

Scanning electrochemical microscopy (SECM) is gaining increasing application in corrosion science for the in situ investigation of localized corrosion processes with high spatial resolution.[1–3] SECM is a scanning probe microscopy (SPM) technique that is based on the amperometric signal generated at a microelectrode by redox-active species in solution, which can perform quantitative local electrochemical experiments at interfaces to gather information on the topography or reactivity of substrates. This is often achieved by applying a variety of electrochemical waveforms at the probe or at the substrate, or even by coupling SECM with other SPM techniques, particularly atomic force microscopy (AFM).[4,5] The SECM probe is often a platinum or gold microelectrode, and by rastering the probe in close proximity to the surface of the sample, a map is made of the substrate properties. In general, image maps formed by SECM are based on an amperometric signal as a function of the tip position. SECM imaging experiments can be performed by either feedback or generation–collection (G–C) mode.[6] SECM has been applied successfully to a great variety of corrosion processes including the visualization of anodic and cathodic areas,[7,8] the identification of precursor sites for pitting corrosion,[9–12] the detection of metastable pit nucleation,[13] the generation of single pits on passive metals,[14–18] the dissolution of inclusions in alloys,[19–21] the water uptake and blister formation at organic-coated metals,[22–24] the degradation of organic coatings from metal–coating interfaces,[25–28] the permeation of hydrogen through metals,[29] and the characterization of chemical inertness of ceramic coatings on metals.[30,31] In most instances, the corrosion process is followed through the detection of the metal ion released in the aqueous phase from the corresponding corroding metal or metal alloy.[25] However, a number of technologically interesting metal materials, such as zinc, cannot be investigated in this way because their corresponding redox potentials are in the range of hydrogen evolution (at about −1.00 V versus $Ag/AgCl/KCl_{sat}$). Interferences can also arise from oxygen reduction, which, for instance, at a Pt-disk microelectrode, produces a single four-electron wave due to the reduction of the oxygen to hydroxide ions at about −0.60 V versus $Ag/AgCl/KCl_{sat}$.[25] Thus, if the redox process to be monitored at the tip occurs at high negative potentials, hydrogen generation or oxygen reduction would hide the signal due to the reduction of the ion species. Another drawback that can be encountered in corrosion investigations performed by

[a] Prof. Dr. R. M. Souto, Dr. Y. González-García
Department of Physical Chemistry
University of La Laguna
38200 La Laguna, Tenerife
Canary Islands (Spain)
Fax: (+34) 922-318002
E-mail: rsouto@ull.es

[b] Dr. D. Battistel, Prof. Dr. S. Daniele
Dipartimento di Scienze Molecolari e Nanosistemi
Università Cà Foscari Venezia
Calle Larga S. Marta, 2137
30123 Venice (Italy)
Fax: (+39) 492-343214683
E-mail: sig@unive.it

SECM coupled to the use of solid microelectrode tips is the circumstance that, for some dissolved metal ions, the only redox process available for detection is the electroreduction to the zero oxidation state. In this case, nucleation and growth of metals on the microelectrode tip leads, in turn, to the continuous modification of the active surface area of the electrode during the measurements. Zinc is an interesting material because metallic structures made of this metal are widely employed in our technological society for a variety of applications, for instance, batteries, die casting, and brass metallurgy, in addition to its common use as galvanized layers for the protection of steel objects. Unfortunately, soluble zinc species cannot be monitored using platinum or other solid microelectrodes in naturally aerated aqueous solutions because their reduction processes are affected by all the aforementioned interferences. This was our motivation for exploring alternate electrode materials to detect zinc ions by SECM during the corrosion process of the metal. To this purpose, an electrode material that possesses useful properties is mercury. In fact, mercury displays high hydrogen overvoltage and forms amalgams with numerous metals. Mercury-coated metal microelectrodes[33] have been extensively used for anodic stripping voltammetry (ASV) of trace metal ions in aqueous solutions.[34–40] More recently, mercury microelectrodes have also been successfully employed as SECM tips to approach solid/solution interfaces to monitor various metal ions, including Zn^{2+}, Cd^{2+}, Pb^{2+}, Cu^{2+}, Mn^{2+}, and Tl^{+}.[41–47] Moreover, the functions to predict diffusion-controlled steady-state currents[48] and approach curves at sphere-cap tips for both negative and positive feedback conditions are available.[49] Mercury sphere-cap microelectrodes can be fabricated onto microdisks of platinum by electrodeposition from mercury-ion solutions; the deposits adopt sphere-cap geometry.[36] Such protruding tips provide a larger electrode area than the basal disks onto which they are fabricated, yet they allow the sample surface to be approached more closely.[42] All these properties make sphere-cap SECM tips very useful for corrosion investigations. However, to the best of our knowledge, only a few papers exist in the literature that deal with the application of Hg-coated Pt SECM tips for investigating the open-circuit release of Cd, Pb, and Bi ions from thin films of the corresponding metals.[47,50] In this paper, we present a study of the corrosion of zinc samples to illustrate the potential of coupling mercury tips and SECM in corrosion science under typical metal-corroding conditions. Naturally aerated aqueous chloride-containing solutions have been employed as the test environment.

Results and Discussion

Monitoring Zn^{2+} ions at mercury microelectrodes: Firstly, the potential ranges for the reduction and the oxidation of zinc species at a mercury microelectrode were tested by cyclic voltammetry in an aerated $Zn(NO_3)_2$ (2 mM) + NaCl (0.1 M) solution. As seen in Figure 1A, in the forward scan, a series of cathodic processes are evident in the potential range that extends from −1.20 to −1.70 V versus Ag/AgCl/KCl_{sat} with a main peak that occurs at −1.50 V versus Ag/AgCl/KCl_{sat}. Over this potential range, the reduction of Zn^{II} species to Zn^0 occurs, as is confirmed by the presence of the anodic peak centered at about −0.80 V versus Ag/AgCl/KCl_{sat}, upon potential reversal. The observation of various peaks during the cathodic scan in the CV can be related to the stepwise reduction of oxygen to hydrogen peroxide [Eq. (1)], the subsequent reduction of hydrogen peroxide to hydroxide anions [Eq. (2)],[51] and the reduction of Zn^{II} species, the process of which is complicated by the formation of sparingly soluble zinc hydroxide or oxide species at the electrode surface.[52] This is due to the high local hydroxide ion concentration induced by the following reactions:

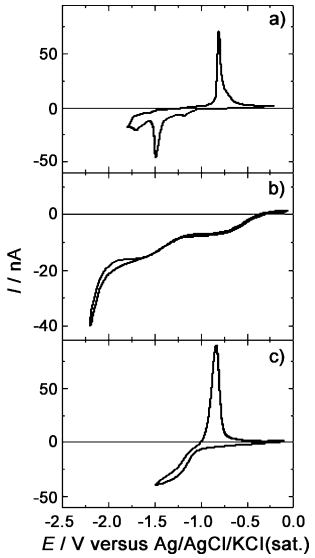

Figure 1. Cyclic voltammograms recorded at a hemispherical mercury microelectrode in A) aerated $Zn(NO_3)_2$ (2 mM) + NaCl (0.1 M) solution ($\nu = 0.05\ V s^{-1}$), B) aerated KNO_3 (0.1 M) solution ($\nu = 0.005\ V s^{-1}$), and C) deaerated $Zn(NO_3)_2$ (2 mM) + NaCl (0.1 M) solution ($\nu = 0.05\ V s^{-1}$). Tip parameters: $a = 25\ \mu m$, $RG = 5$, $H = 1$.

$$O_2 + 2\,H_2O + 2e^- \rightarrow H_2O_2 + 2\,OH^- \quad (1)$$

$$H_2O_2 + 2e^- \rightarrow 2\,OH^- \quad (2)$$

The formation of sparingly soluble compounds at the electrode surface would explain the presence of a reduction peak instead of a wave, as expected for microelectrodes that work on an experimental timescale in which hemispherical diffusion prevails.[53] To confirm this scenario, CV measurements were performed either in a NaCl (0.1 M) aerated solution in the absence of Zn^{II} ions (Figure 1B) or in a deoxygenated $Zn(NO_3)_2$ (2 mM) + NaCl (0.1 M) solution (Figure 1C). As is evident from Figure 1B, in the aerated solution two well-defined waves that correspond to Equations (1) and (2)[43] are observed. This supports the idea that Zn^{II} ions are actually reduced in a locally basic medium. On the other hand, as is shown in Figure 1C, the shape of the

CV is simpler when the experiment was performed in the same electrolyte solution (as in Figure 1A) after purging with nitrogen. In fact, when dissolved oxygen molecules had been removed from the electrolyte, the expected sigmoidal reduction wave in the cathodic scan (characterized by a half-wave potential of −1.10 V versus Ag/AgCl/KCl_{sat}) and the stripping peak due to oxidation of metallic Zn is observed. Measurements carried out in the bulk Zn^{2+}-containing solution after purging with nitrogen for different times so as to vary the amount of oxygen present in the medium provided CVs of a shape that varied between those of Figure 1A and C, which move from high to low oxygen content. These preliminary experiments therefore suggested that: 1) oxygen could be monitored in a CV scan that corresponded to the first wave in Figure 1B with no interference from Zn^{II} ions, and 2) Zn^{II} ions could be monitored at more negative potentials through either the plateau current in the negative scan (if the amount of oxygen locally present is low) or from the stripping peak in the reverse potential scan for low zinc-ion concentration or in solutions that contain relatively high oxygen concentration.

Zinc metal-corrosion processes during exposure to aqueous chloride solution: The possibility of monitoring independently the release of zinc(II) species during the corrosion of the metal and the simultaneous oxygen depletion by the use of the mercury microelectrode as an SECM tip was next investigated through the exposure of a pure zinc sample to naturally aerated NaCl (0.1 M) solutions. The zinc sample was kept unbiased throughout the experiments. Figure 2 contrasts typical approach curves recorded either on the insulating material that surrounded the zinc surface or that performed at the sample surface by setting the tip potential at −0.70 V versus Ag/AgCl/KCl_{sat}, where only the reduction of oxygen occurred through Equation (1). Above the insulating substrate, negative feedback is observed, which reflects the decrease in the normalized current with the decrease of the tip–substrate distance due to the partial blockage of oxygen diffusion to the microelectrode.[6,43] Above the zinc surface, negative feedback is also recorded. However, in the latter case, oxygen depletion starts at higher tip–substrate distances. This clearly reflects the consumption of oxygen at the zinc surface during the corrosion, and it represents the oxygen diffusion layer thus established. The generation of Zn^{2+} ions was recorded by using a different procedure. The experiments consisted of recording a series of CVs at 50 mV s^{-1} over the potential range from 0 to −1.60 V versus Ag/AgCl/KCl_{sat} by placing the mercury microelectrode tip at varying distances from the spontaneously corroding metal. It was observed that far away from the substrate the CVs closely resembled that displayed in Figure 1B for oxygen reduction alone. On the other hand, when moving the tip towards the substrate, the CV shapes transitioned from that shown in Figure 1A to that displayed in Figure 1C at relatively small tip–substrate distances. Whenever possible, plateau currents were then determined from each voltammogram, and the values were plotted as a function of the tip–sample distance as is shown in Figure 3A. It is observed that the values of the limiting current greatly increase as the microelectrode approaches the metal surface, this effect being noticeable for tip–sample distances smaller than 400 μm, as should be expected for a corroding metal that acts as the source of the zinc ions. On the other hand, when the tip is located far away from the zinc sample (that is, for tip–sample distances greater than 500 μm under the

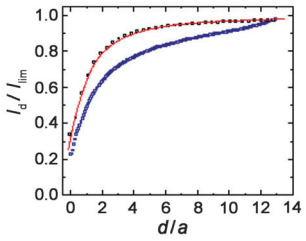

Figure 2. Approach curves recorded with the Hg microelectrode immersed in NaCl (0.1 M) aerated solution above the insulating surface (□) or above the zinc sample (□). Tip potential: −0.70 V versus Ag/AgCl/KCl_{sat}; scan rate: 10 μm s^{-1}. (——) Theoretical approach curve calculated for negative feedback condition at a sphere-cap microelectrode with $H=1$ and $RG=5$.

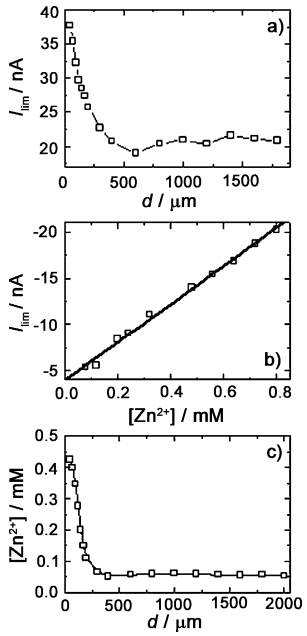

Figure 3. A) Diffusion-limiting current at the hemispherical mercury microelectrode as a function of the tip–sample distance. The values were obtained from the linear voltammetric curves measured by placing the microelectrode at various distances from the sample. B) Calibration plot for Zn^{II} ions measured with the Hg microelectrode in NaCl (0.1 M) solution containing different amounts of $Zn(NO_3)_2$. C) Concentration profile of the dissolving Zn^{II} species expressed as a function of the distance between the mercury microelectrode and the zinc sample.

employed experimental conditions), the limiting currents determined from the voltammograms never became zero. A value of about (20±2) nA was always found regardless of the distance of the tip from the corroding sample. This non-zero current arose from the reduction of the dissolved oxygen in the electrolyte, which thus constitutes a background current that adds to the Faradaic signal detected at the tip during the CV measurements for Zn^{II} reduction. This signal must be subtracted from the total current if the actual contribution of metal ions to the current measured at the tip is to be determined. As an approximate method, the limiting current measured at the SECM probe in the CVs was related to the concentration of Zn^{2+} by using an external calibration plot performed in a deoxygenated NaCl (0.1 M) solution. As is shown in Figure 3B, the plateau current was found to depend linearly on the concentration of Zn^{II} over the range 0.05–0.8 mM, which was wide enough to establish the amount of Zn^{II} generated during the corrosion process. Thus, after the background current in the current values of Figure 3A was subtracted, a relationship between the concentrations of dissolved Zn^{II} ions as a function of the tip–sample distance could be estimated as shown in Figure 3C. It must be remarked that the approach curves recorded either for oxygen or zinc ions (with the above procedures) depended on the actual position of the tip above the substrate as well as on the time the substrate had been left immersed in the aerated solution, as the corrosion process starts as soon as the sample comes into contact with the aerated solution. The latter circumstances explain the reasons why in the above experiments the distances at which oxygen depletion started to occur or zinc ions could be detected were different.

SECM mapping of zinc metal-corrosion processes: The corrosion of zinc metal during immersion in an aqueous solution that contained chloride anions led to the release of Zn^{II} ions as a result of the anodic process, whereas the dissolved oxygen is reduced in the cathodic process (see Scheme 1). The metal ions or molecular oxygen can be detected by using the mercury microelectrode tip as shown in the previous section. In this way, SECM scans performed across the sample can visualize the distribution of anodic and cathodic sites distributed on the metal exposed to the corrosive environment. The operating tip–sample distance for SECM operation was established after recording approach curves of the microelectrode tip towards the insulating epoxy sleeve that surrounded the metal specimen. The potential of the tip was set at −0.70 V versus $Ag/AgCl/KCl_{sat}$ to use oxygen electroreduction as redox mediator,[54] and a negative feedback effect resulted as the microelectrode approached the sample. After the tip was retracted to a height of 50 μm, which was considered a suitable distance to avoid tip damage, either SECM line scans or two-dimensional scans were registered above the zinc specimen. From the cyclic voltammograms displayed in Figure 1, a suitable potential for the reduction of zinc ions to Zn(Hg) was established. We adopted a tip potential value of −1.20 V versus $Ag/AgCl/KCl_{sat}$. At this potential, in the absence of Zn^{II} ion species the reduction of oxygen that corresponded to the first wave could be monitored as well. Figure 4 shows the steady-state currents monitored at the microelectrode during a line scan taken through the center of the zinc specimen (the metal is located between 250 and 1250 μm). It is evident that when the microelectrode reaches the *X* value of 250 μm (that is, the border of the metal surface), the current measured at the tip starts to increase over the background current values. A rather symmetric current peak is defined as the tip is displaced further over the zinc specimen; then the tip Faradaic current falls below even the background currents to describe another current peak that extends over longer distances than the previous ones. The first current peak, which presents the greatest values of the cathodic current, is conceivably due to the electroreduction of Zn^{II} ions released by the corroding metal at the anodic sites. That is, the SECM tip was actually monitoring the flow of Zn^{II} species from the dissolving surface of zinc towards the bulk solution. Supplementary evidence for this hypothesis is gathered from inspection of the cyclic voltammogram shown in Figure 5, which was recorded after placing the microelectrode tip above the place on the surface of the metal, at

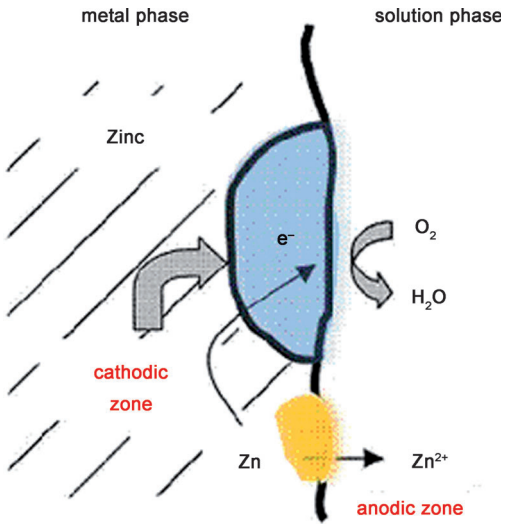

Scheme 1. Illustration of the corrosion processes taking place on the surface of zinc metal during exposure to a chloride-containing environment.

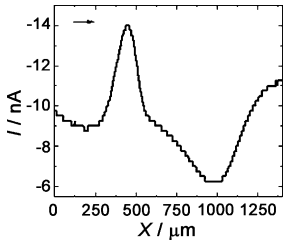

Figure 4. Illustration of the corrosion processes taking place on the surface of zinc metal during exposure to a chloride-containing environment.

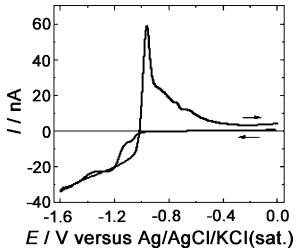

Figure 5. Cyclic voltammogram recorded at the Hg microelectrode located above the place on the surface of the metal at which point a current peak is observed during the line scan shown in Figure 6; $\nu = 0.05\ V\,s^{-1}$, tip/substrate distance: 50 μm.

which point a current peak was observed during the line scan shown in Figure 4, while keeping it at the same height. The characteristic wave during the negative scan and the anodic peak after scan reversal can be observed, as expected for the Zn^{II}/Zn^{0} reduction/oxidation at the Hg microelectrode. As for the second peak observed in the line scan recorded in Figure 4, the following considerations can be made. If zinc were homogeneously corroding, the tip would have recorded bigger cathodic currents than the background values as long as the tip passed above the metal surface. Instead there is a region over the zinc sample at which a depletion of cathodic current is observed. This result indicates that two zones with different electrochemical behaviors were found while the tip was rastering the surface of the metal. The development of areas on the zinc sample for which the microelectrode tip polarized at −1.20 V versus $Ag/AgCl/KCl_{sat}$ recorded smaller cathodic values than the background current is related to the cathodic half-reaction in the corrosion process. Indeed, two different redox reactions can simultaneously occur at the tip at this potential, namely: 1) the reduction of the Zn^{II} to Zn, and 2) the reduction of the oxygen (see the cyclic voltammogram of oxygen using the Hg electrode given in Figure 1B). Therefore, the observed decrease in current during the line scan could arise from local areas at the metal surface in which oxygen was consumed during the cathodic reaction. The tip would thus detect lower amounts of dissolved oxygen in the solution in the proximity of the cathodic sites. Additional support for this interpretation is given by Figure 6. It depicts the line scan recorded when the potential at the tip, set at −0.7 V versus $Ag/AgCl/KCl_{sat}$, was passing above the same line of the sample covered in Figure 4. In this case, only the area of depleted currents below the background was observed. This agrees well with the expectation that the only redox process that could occur at the microelectrode at this potential is the reduction of oxygen. It is also interesting to notice that the depletion of the current in Figure 6 occurred precisely above the same region of the zinc sample in which depleted currents were recorded at the microelectrode biased at −1.20 V versus $Ag/AgCl/KCl_{sat}$ previously shown in Figure 4. The extent and location of the different active areas on the zinc sample during its exposure to the test solution could be imaged by acquiring a two-dimensional scan of the metal surface with the tip polarized at −1.20 V versus Ag/AgCl/KCl. The resulting 3D image is shown in Figure 7. A narrow peak that exhibits rather high negative currents is clearly displayed, and this is due to the electroreduction of the dissolving Zn^{II} ions from the sample. Next, a rather extended area with depleted currents is found in the proximity of the anodic peak, an indirect observation of the cathodic reaction contribution to the overall corrosion reaction. In this way, mercury microelectrodes polarized at −1.20 V versus $Ag/AgCl/KCl_{sat}$ allow for the detection of both anodic and cathodic sites from the observation of larger and smaller reduction currents at the tip than the background values measured over the insulator. This procedure was employed to monitor the temporal evolution of the electrochemical activity on the zinc substrate by recording a sequence of SECM images as shown in Figure 8. It is observed that anodic activity changes location and intensity over time due to the progressive blockage of the initial anode by corrosion products. This situation eventually leads to the formation of a new anode at a different location on the metal surface to support the oxidation of the metal. Anodic activity always occurs in a highly localized manner on the metal surface, that is, the area of the anodes is small. Conversely, the cathodic reaction extends over most of the surface of the exposed specimen.

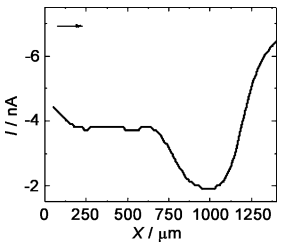

Figure 6. Line scan of a hemispherical mercury microelectrode travelling above the zinc surface after immersion in NaCl (0.1 M). Tip potential: −0.70 V versus $Ag/AgCl/KCl_{sat}$, tip/substrate distance: 50 μm. The arrow indicates the direction of tip movement.

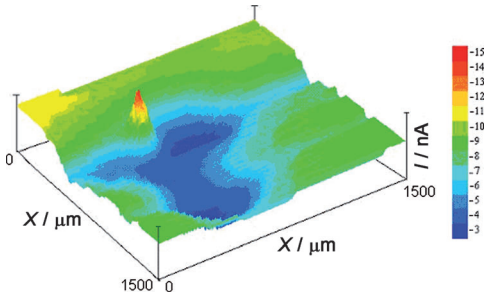

Figure 7. SECM 3D map taken above a zinc sample immersed in NaCl (0.1 M) recorded by using a hemispherical Hg microelectrode. Tip potential: −1.20 V versus $Ag/AgCl/KCl_{sat}$), tip/substrate distance: 50 μm, scan rate: 37 $\mu m\,s^{-1}$.

Conclusion

The use of hemispherical mercury microelectrodes as the scanning probe in SECM can be used to detect the zinc(II) ions released in the corrosion of zinc specimens immersed in

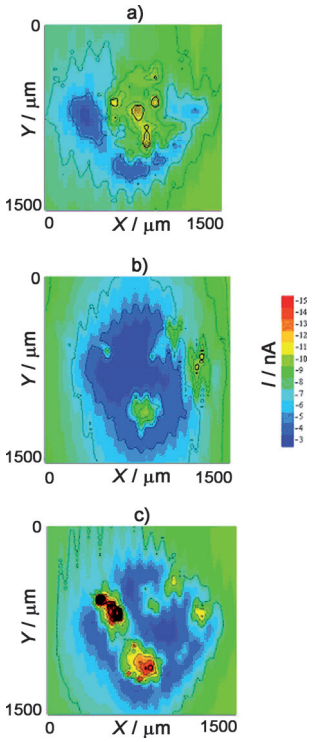

Figure 8. Two-dimensional scans above a zinc sample immersed in NaCl (0.1 M) recorded by using a hemispherical Hg microelectrode recorded at different exposure times: A) 1, B) 18, and C) 24 h. Tip potential: −1.20 V versus Ag/AgCl/KCl_{sat}, tip/substrate distance: 50 µm, scan rate: 37 µm s^{-1}.

an aggressive solution at the open-circuit potential. Adequate selection of the tip polarization potential allows the zinc-reduction current to be effectively separated from the total current measured at the microelectrode. By setting the potential of the Hg microelectrode to −1.20 V versus Ag/AgCl/KCl_{sat}, both the Zn^{II} ions that originate from the electro-dissolution of zinc at the anodic sites on the metal surface, and the depletion of oxygen in the electrolyte in the proximity of the corresponding cathodic sites could be detected. The development of two separated zones with different electrochemical behaviors could thus be distinguished as the tip rastered the surface of the metal. The anodic sites on the zinc specimen give rise to enhanced cathodic currents at the microelectrode compared to the steady-state limiting current, and the SECM tip was actually monitoring the flow of Zn^{II} species from the dissolving surface of zinc. Indirect detection of the cathodic reaction was also achieved from those areas at the zinc surface that originated depleted currents at the tip compared to the steady-state limiting current. They were found in the proximity of the anodic areas, because the tip effectively detected lower concentrations of the dissolved oxygen in the solution close to those sites. That is, both the anodic and cathodic reactions responsible for the corrosion process were located over the same metal. Concentration profiles of dissolved zinc species that originate from the corroding metal could be determined by using simple CVs at the Hg-microelectrode tip for different tip–substrate distances. It was shown that, as expected, greater concentrations of Zn^{II} species were observed as the microelectrode was brought nearer to the surface of the metal.

Experimental Section

Solutions and samples: All chemicals employed were of analytical reagent grade and used as received. NaCl, KCl, and ruthenium(III) hexaammine trichloride were purchased from Aldrich; $Hg_2(NO_3)_2$ and KNO_3 were purchased from Fluka. Titrisol zinc atomic absorption standard (Merck) was used to prepare stock standard solutions (1000 mg L^{-1}) of the metal ions. All solutions were prepared by using water purified using a Milli-Q system (Millipore, Bedford, MA). Measurements that required no oxygen were carried out in solutions that had been purged with pure nitrogen (99.99%) purchased from SIAD (Bergamo, Italy). Corrosion experiments were performed on 99.95% pure zinc supplied as sheets of thickness 1 mm by Goodfellow Materials Ltd (Cambridge, UK). The sheets were cut to squares of about 1×1 mm^2 to form the testing metal substrates, and they were embedded into an epoxy resin sleeve, such that only the square-end surface formed the testing surface. The mounts with the samples were polished with silicon carbide paper down to 1200 grit, washed thoroughly with Millipore deionized water, dried with acetone, and finally surrounded laterally by Sellotape, thus creating a small container for the test electrolyte solution. Tests were carried out in aqueous NaCl (0.1 M) solution. For the calibration of the mercury microelectrodes for zinc detection, solutions that contained controlled amounts of $Zn(NO_3)_2$ were produced by addition of the salt to the base electrolyte. All aqueous solutions were prepared with analytical-reagent-grade chemicals and Milli-Q water. The solutions were naturally aerated, and experiments were performed at ambient temperature, which was (21±1) °C.

Electrodes and instrumentation: The platinum microdisks, which served as the substrate for mercury deposition, were prepared by sealing wires 25 µm in diameter into glass capillaries. The electrode tips were then laterally polished with silicon carbide paper of different grits to produce a conical shape. Prior to mercury deposition, the exposed microdisks were polished with graded alumina powder of different sizes on a polishing microcloth. The effective electrode radius (a) of the exposed microdisks were characterized by cyclic voltammetry at low scan rates in deaerated $[Ru(NH_3)_6Cl_3]$ (1 mM) + KCl (0.1 M) solution by determining the steady-state limiting currents (I_{lim}) for the one-electron reduction of $[Ru(NH_3)_6]^{3+}$ ($D=7\times10^{-6}$ cm^2s^{-1})[30,32] while the electrode was held in the bulk solution. Negative-feedback current approach curves (that is, normalized currents, I_d/I_{lim}, against normalized tip/substrate distance, d/a) obtained with these tips fit well the theory for RG[6], the ratio of the radius of the tip (electrode plus surrounding insulator, r_g) to that of the electrode itself, equal to 5. Deposition of mercury onto the above-characterized platinum microdisks was carried out under potentiostatic control by setting the microelectrode potential at −0.10 V versus Ag/AgCl/KCl_{sat} in $Hg_2(NO_3)_2$ (5 mM) + KNO_3 (0.1 M) acidified to pH 1 with HNO_3.[37] The size of the mercury sphere caps thus produced was controlled by measuring the charge spent during the electrodeposition step from the corresponding chronoamperometric curve. The mercury microelectrode aspect ratio, described by the parameter $H=h/a$, that is, the ratio of the sphere-cap height (h) to the basal radius of the electrode (a) was obtained from the steady-state limiting current recorded in deaerated $[Ru(NH_3)_6Cl_3]$ (1 mM) + KCl (0.1 M) solution by using the method described in ref. [48]. Mercury microelectrodes with H over the range 0.98–1.09 were employed. The stability of the Hg tips during the SECM measurements was ascertained by comparing the cyclic voltammograms at low scan rates performed in the $[Ru(NH_3)_6Cl_3]$ solution before and after the SECM measurements. The electrode geometry and its stability were also confirmed by performing approach curves above an insulating substrate in the $[Ru(NH_3)_6Cl_3]$ solution. The curve was fitted to the theoretical function for hindered diffusion to a microsphere cap[42] characterized by parameters $H=1$ and $RG=5$. A home-built SECM apparatus (previously described in ref. [42]) was employed. Cyclic voltammetry (CV) and chronoamperometry were performed using a PAR 283 potentiostat/galvanostat controlled with a personal computer and the M270 PAR software.

All measurements were carried out in a classical three-electrode cell arrangement located in a Faraday cage.

Acknowledgements

The authors are grateful to the Spanish Ministry of Science and Innovation (MICINN, Madrid) and the Italian Ministry of Universities and Research (MIUR, Rome) for the grant of a Collaborative Research Programme between Spain and Italy (Acción Integrada no. HI2004-0297) to fund this work. The Ministerio de Ciencia e Innovación (Madrid, Spain) and the European Regional Development Fund (Brussels, Belgium) assisted in meeting the publication costs of this article under grant no. CTQ2009-12459/PPQ. Y.G.G. is grateful to the University of La Laguna and Cajacanarias for the award of a doctoral grant.

[1] S. E. Pust, W. Maier, G. Wittstock, *Z. Phys. Chem. (Muenchen Ger.)* **2008**, *222*, 1463–1517.
[2] L. Niu, Y. Yin, W. Guo, M. Lu, R. Qin, S. Chen, *J. Mater. Sci.* **2009**, *44*, 4511–4521.
[3] R. M. Souto, S. Lamaka, S. González in *Microscopy: Science Technology, Applications and Education, Vol. 3* (Eds.: A. Méndez-Vilas, J. Díaz), Formatex Research Center, Badajoz, **2010**, 1769–1780.
[4] A. Davoodi, J. Pan, C. Leygraf, S. Norgren, *Electrochim. Acta* **2007**, *52*, 7697–7705.
[5] A. Davoodi, J. Pan, C. Leygraf, S. Norgren, *J. Electrochem. Soc.* **2008**, *155*, C211–C218.
[6] *Scanning Electrochemical Microscopy* (Eds.: A. J. Bard, M. V. Mirkin), Marcel Dekker, New York, **2001**.
[7] A. C. Bastos, A. M. Simões, S. González, Y. González-García, R. M. Souto, *Electrochem. Commun.* **2004**, *6*, 1212–1215.
[8] A. M. Simões, A. C. Bastos, M. G. Ferreira, Y. González-García, S. González, R. M. Souto, *Corros. Sci.* **2007**, *49*, 726–739.
[9] Y. Y. Zhu, D. E. Williams, *J. Electrochem. Soc.* **1997**, *144*, L43–L45.
[10] S. B. Basame, H. S. White, *J. Phys. Chem. B* **1998**, *102*, 9812–9819.
[11] L. F. Garfias-Mesias, M. Alodan, P. I. James, W. H. Smyrl, *J. Electrochem. Soc.* **1998**, *145*, 2005–2010.
[12] M. A. Malik, P. J. Kulesza, G. Pawlowska, *Electrochim. Acta* **2009**, *54*, 5537–5543.
[13] Y. González-García, G. T. Burstein, S. González, R. M. Souto, *Electrochem. Commun.* **2004**, *6*, 637–642.
[14] D. O. Wipf, *Colloid Surf. A* **1994**, *93*, 251–261.
[15] K. Fushimi, M. Seo, *J. Electrochem. Soc.* **2001**, *148*, B450–B456.
[16] F. Falkenberg, K. Fushimi, M. Seo, *Corros. Sci.* **2003**, *45*, 2657–2670.
[17] C. Gabrielli, S. Joiret, M. Keddam, H. Perrot, N. Portail, P. Rousseau, V. Vivier, *Electrochim. Acta* **2007**, *52*, 7706–7714.
[18] C. Gabrielli, S. Joiret, M. Keddam, N. Portail, P. Rousseau, V. Vivier, *Electrochim. Acta* **2008**, *53*, 7539–7548.
[19] C. H. Paik, H. S. White, R. C. Alkire, *J. Electrochem. Soc.* **2000**, *147*, 4120–4124.
[20] D. E. Williams, Y. Y. Zhu, *J. Electrochem. Soc.* **2000**, *147*, 1763–1766.
[21] C. H. Paik, R. C. Alkire, *J. Electrochem. Soc.* **2001**, *148*, B276–B281.
[22] R. M. Souto, Y. González-García, S. González, G. T. Burstein, *Corros. Sci.* **2004**, *46*, 2621–2628.
[23] R. M. Souto, Y. González-García, S. González, *Corros. Sci.* **2008**, *50*, 1637–1643.
[24] R. M. Souto, Y. González-García, S. González, G. T. Burstein, *Electroanalysis* **2009**, *21*, 2569–2574.
[25] R. M. Souto, Y. González-García, S. González, *Corros. Sci.* **2005**, *47*, 3312–3323.
[26] J. J. Santana, J. González-Guzmán, L. Fernández-Mérida, S. González, R. M. Souto, *Electrochim. Acta* **2010**, *55*, 4488–4494.
[27] A. M. Simoes, D. Battocchi, D. E. Tallman, G. P. Bierwagen, *Corros. Sci.* **2007**, *49*, 3838–3849.
[28] Y. González-García, J. M. C. Mol, T. Muselle, I. De Graeve, G. Van Assche, G. Scheltjens, B. Van Mele, H. Terryn, *Electrochem. Commun.* **2011**, *13*, 169–173.
[29] S. Modiano, J. A. V. Carreño, C. S. Fugivara, R. M. Torresi, V. Vivier, A. Benedetti, O. R. Mattos, *Electrochim. Acta* **2008**, *53*, 3670–3679.
[30] D. Battistel, S. Daniele, G. Battaglin, M. A. Baldo, *Electrochem. Commun.* **2009**, *11*, 2195–2198.
[31] D. A. Walsh, L. E. Li, M. S. Bakare, K. T. Voisey, *Electrochim. Acta* **2009**, *54*, 4647–4654.
[32] D. Battistel, S. Daniele, R. Gerbasi, M. A. Baldo, *Thin Solid Films* **2010**, *518*, 3625–3631.
[33] L. C. R. Alfred, K. B. Oldham, *J. Phys. Chem.* **1996**, *100*, 2170–2177.
[34] A. S. Baranski, H. Quon, *Anal. Chem.* **1986**, *58*, 407–412.
[35] S. Daniele, G. A. Mazzochin, *Anal. Chim. Acta* **1993**, *273*, 3–11.
[36] M. Ciszkowska, M. Donten, Z. Stojek, *Anal. Chem.* **1994**, *66*, 4112–4115.
[37] M. A. Baldo, S. Daniele, M. Corbetta, G. A. Mazzochin, *Electroanalysis* **1995**, *7*, 980–986.
[38] M. A. Baldo, S. Daniele, G. A. Mazzochin, *Anal. Chim. Acta* **1997**, *340*, 77–87.
[39] F. Zhou, J. T. Aronson, M. W. Ruegnitz, *Anal. Chem.* **1997**, *69*, 728–733.
[40] S. Daniele, M. A. Baldo, C. Bragato, *Curr. Anal. Chem.* **2008**, *4*, 215–228.
[41] S. Daniele, C. Bragato, I. Ciani, M. A. Baldo, *Electroanalysis* **2003**, *15*, 621–628.
[42] I. Ciani, S. Daniele, C. Bragato, *Electrochem. Commun.* **2003**, *5*, 354–358.
[43] S. Daniele, I. Ciani, M. A. Baldo, C. Bragato, *Electroanalysis* **2007**, *19*, 2067–2076.
[44] M. Janotta, D. Rudolph, A. Kueng, C. Kranz, H. S. Voraberger, W. Waldhauser, B. Mizaikoff, *Langmuir* **2004**, *20*, 8634–8640.
[45] D. Rudolph, S. Neuhuber, C. Kranz, M. Taillefert, B. Mizaikoff, *Analyst* **2004**, *129*, 443–448.
[46] J. Mauzeroll, M. Buda, A. J. Bard, F. Prieto, M. Rueda, *Langmuir* **2002**, *18*, 9453–9461.
[47] M. A. Alpuche-Aviles, J. E. Baur, D. O. Wipf, *Anal. Chem.* **2008**, *80*, 3612–3621.
[48] S. Daniele, I. Ciani, D. Battistel, *Anal. Chem.* **2008**, *80*, 253–259.
[49] G. Lindsey, S. Abercrombie, G. Denuault, S. Daniele, E. De Faveri, *Anal. Chem.* **2007**, *79*, 2952–2956.
[50] M. O. Salles, D. Battistel, A. S. Lima, M. Bertotti, S. Daniele, *Electroanalysis* **2011**, *23*, 595–603.
[51] D. Pletcher, S. Sotiropoulos, *J. Chem. Soc. Faraday Trans.* **1995**, *91*, 457–462.
[52] Th. Pauporté, D. Lincot, *J. Electroanal. Chem.* **2001**, *517*, 54–62.
[53] M. A. Baldo, S. Daniele, G. A. Mazzocchin, *Electrochim. Acta* **1996**, *41*, 811–818.
[54] C. Bragato, S. Daniele, M. A. Baldo, G. Denuault, *Ann. Chim.* **2002**, *92*, 153–161.

Received: July 27, 2011
Published online: November 30, 2011

